Inorganic Chemistry

Article

pubs.acs.org/IC

Lanthanide Complexes Based on a Diazapyridinophane Platform Containing Picolinate Pendants

Adrián Roca-Sabio,[†] Célia S. Bonnet,[‡] Marta Mato-Iglesias,[†] David Esteban-Gómez,[†] Éva Tóth,[‡] Andrés de Blas,[†] Teresa Rodríguez-Blas,*[,†] and Carlos Platas-Iglesias*[,†]

[†]Departamento de Química Fundamental, Facultade de Ciencias, Universidade da Coruña, Campus da Zapateira, Rúa da Fraga 10, 15008 A Coruña, Spain

[‡]Centre de Biophysique Moléculaire, CNRS, rue Charles-Sadron, 45071 Orléans, Cedex 2, France

Supporting Information

ABSTRACT: A new macrocyclic ligand, *N*,*N*′-bis[(6-carboxy-2-pyridyl)methyl]-2,11-diaza[3.3](2,6)pyridinophane (H_2BPDPA), was prepared, and its coordination properties toward the Ln^{III} ions were investigated. The hydration numbers (q) obtained from luminescence lifetime measurements in aqueous solution of the Eu^{III} and Tb^{III} complexes indicate that they contain one inner-sphere water molecule. The structure of the complexes in solution has been investigated by ^{1}H and ^{13}C NMR spectroscopy, as well as by theoretical calculations performed at the density functional theory (B3LYP) level. The minimum-energy conformation calculated for the Yb^{III} complex is in excellent agreement with the experimental structure in solution, as demonstrated by analysis of the Yb^{III}-induced paramagnetic ^{1}H shifts. Nuclear magnetic relaxation dispersion (NMRD) profiles and ^{17}O NMR measurements recorded on solutions of the Gd^{III} complex were used to determine the parameters governing the relaxivity. The results show that this system is endowed with a relatively fast water-exchange rate $k_{ex}^{298} = 63 \times 10^6$ s^{-1}. Thermodynamic stability constants were determined by pH-potentiometric titration at 25 °C in 0.1 M KCl. The stability constants, which fall within the range $\log K_{LnL} = 12.5-14.2$, point to a relatively low stability of the complexes primarily as a consequence of the low basicity of the ligand.

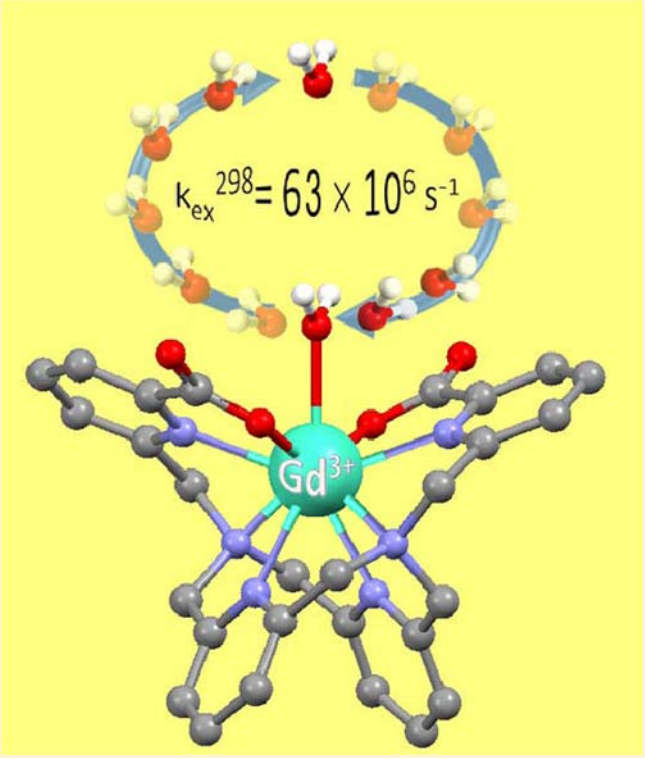

INTRODUCTION

Ln^{III} complexes with poly(aminocarboxylate) ligands are receiving considerable interest because of their successful application in different imaging modalities. Indeed, luminescent lanthanide complexes offer exceptional photophysical properties that find applications in different fields such as biomedical analyses and imaging,[1] while Gd^{III} complexes are currently used in vivo as contrast agents in magnetic resonance imaging (MRI).[2,3] Application of Ln^{III} complexes in these fields requires an efficient complexation of the metal ion, with suitable ligands ensuring a high stability to prevent the release of the toxic-free metal ion.[4,5] This is normally achieved with the use of poly(aminocarboxylate) ligands based on either linear or macrocyclic frameworks, although macrobicyclic ligands such as the famous Lehn cryptands have also been successfully used for in vitro bioanalytical applications.[6] In general, macrocyclic ligands form Ln^{III} complexes with superior kinetic stabilities compared to nonmacrocyclic derivatives.[5]

Besides a high stability in biological media, luminescent lanthanide complexes for biological application must contain adequate chromophoric units to collect the excitation photons and provide an efficient energy transfer to populate the Ln^{III} ion excited state (antenna effect[7]). It is well-known that OH oscillators of coordinated water molecules provide an efficient pathway for the radiationless deactivation of the Ln^{III}-centered excited states.[8] Thus, the design of efficient luminescent Ln^{III}-based labels requires an adequate protection of the metal-ion coordination environment to avoid the coordination of water molecules. On the other hand, stable Gd^{III} chelates for

Received: June 26, 2012
Published: September 27, 2012

application as MRI contrast agents must contain at least one Gd^{III}-bound water molecule that rapidly exchanges with the bulk water of the body, thereby imparting an efficient mechanism for the longitudinal and transverse relaxation enhancement ($1/T_1$ and $1/T_2$) of water protons.[9,10] The efficiency of a contrast agent in vitro is measured in terms of its relaxivity,[11] which is defined as the relaxation-rate enhancement of water protons per millimolar concentration of metal ion. In spite of these apparently noncompatible requirements, it has been shown that certain Ln^{III} complexes present relatively high luminescence quantum yields of the Ln^{III}-centered luminescence and high relaxivities,[12] thereby paving the way for the design of bimodal (MRI/optical imaging) probes coupling the high sensitivity of luminescence and the high resolution of MRI.[13] In previous works, Mazzanti et al. demonstrated that ligands containing picolinate moieties can act as antennas to sensitize the emission of both Eu^{III} and Tb^{III} with excellent quantum yields.[14] Furthermore, some ligands containing picolinate units were shown to provide Gd^{III} complexes with high thermodynamic stabilities.[14,15] Macrocyclic ligands often form Ln^{III} complexes with higher thermodynamic and kinetic stabilities than the nonmacrocyclic analogues. Thus, macrocyclic ligands containing picolinate pendant arms are promising candidates for the development of bimodal probes for MRI and optical imaging.

In recent papers, we reported a series of macrocyclic ligands containing picolinate pendants that showed interesting relaxation properties. $[Gd(BP12C4)]^+$ (Chart 1) was found

Chart 1

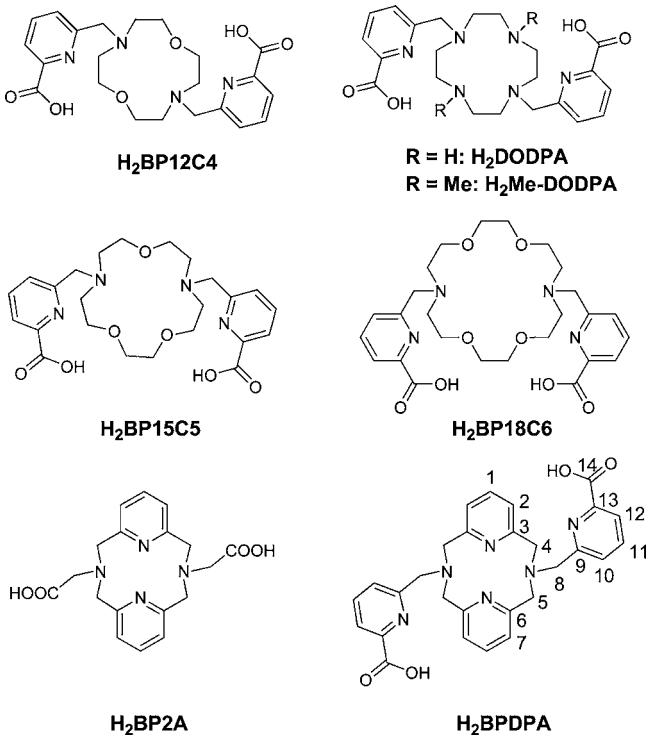

to exist in solution as a mixture of mono- and bishydrated species, with an average hydration number q of 1.4 at 298 K.[16] The inner-sphere water molecules are endowed with a very fast water-exchange rate (k_{ex}^{298} = 220 × 10^6 s^{-1}), with the water-exchange reaction following an associative exchange mechanism.[17] This complex was also found to possess a relatively high stability (log K_{Gd} = 18.8, 25 °C, 0.1 M KCl) and a slightly higher kinetic stability than complexes with nonmacrocyclic ligands such as $[Gd(DTPA)]^{2-}$.[17] The q value estimated for $[Gd(DODPA)]^+$ from luminescence lifetime measurements on the Eu^{III} and Tb^{III} analogues was somewhat lower (q = 0.8), while the water-exchange rate was found to be also rather fast (k_{ex}^{298} = 58 × 10^6 s^{-1}).[18] The higher water-exchange rate observed for $[Gd(BP12C4)]^+$ compared to $[Gd(DODPA)]^+$ is probably related to a more important degree of flexibility of the metal-ion coordination environment in the former.[19] Unexpectedly, the introduction of methyl groups in positions 4 and 10 of the cyclen unit to give $[Gd(Me\text{-}DODPA)]^+$ increased the steric compression around the water binding site, which resulted in q = 0 complexes.[18]

In this contribution, we report a new macrocyclic ligand derived from a diazapyridinophane platform that contains two picolinate pendant arms (H_2BPDPA, Chart 1). Considering that $BP12C4^{2-}$, $DODPA^{2-}$, and $BPDPA^{2-}$ possess analogous ligand topologies, these ligands are expected to provide Ln^{III} complexes with similar properties. However, the presence of a very rigid diazapyridinophane unit is likely to have an impact on the stability of the complexes, as well as on the water exchange of the inner-sphere water molecule(s). Thus, the thermodynamic stability of the Ln^{III} complexes of $BPDPA^{2-}$ has been investigated by using potentiometric titrations. The photophysical properties of the Eu^{III} and Tb^{III} complexes have been investigated to determine the hydration number of the complexes in solution and the quantum yields of the metal-centered luminescence. Nuclear magnetic relaxation dispersion (NMRD) investigations and variable-temperature ^{17}O NMR measurements of the Gd^{III} complex were performed in order to assess its ^1H relaxation enhancement abilities and to gain insight into the parameters governing the relaxivity. Additionally, the structures of the complexes in solution have been investigated by using ^1H and ^{13}C NMR techniques in a D_2O solution and density functional theory (DFT) calculations. The structure established by these calculations was compared with the structural information obtained in solution from paramagnetic NMR measurements (Yb^{III}-induced ^1H NMR shifts).

EXPERIMENTAL SECTION

Physical Methods. Elemental analyses were carried out on a Carlo Erba 1108 elemental analyzer. Electrospray ionization time-of-flight (ESI-TOF) mass spectra were recorded using a LC-Q-q-TOF Applied Biosystems QSTAR Elite spectrometer in the positive mode. UV−vis spectra were recorded on a Perkin-Elmer Lambda 900 spectrophotometer in 1.0-cm-path-length quartz cells. Excitation and emission spectra were recorded on a Perkin-Elmer LS-50B spectrometer. Luminescence lifetimes were calculated from the monoexponential fitting of the average decay data, and they are averages of at least three to five independent determinations. Luminescence quantum yields were measured according to conventional procedures,[20] with diluted solutions (optical density < 0.05), using $[Ru(bipy)_3]Cl_2$ in nondegassed water (Φ = 2.8%)[21] and rhodamine 6G in water (Φ = 76% at λ_{exc} = 488 nm),[22] with an estimated error of ±15%. ^1H and ^{13}C NMR spectra were recorded at 25 °C on Bruker Avance 300 and Bruker Avance 500 MHz spectrometers. For measurements in D_2O, *tert*-butyl alcohol was used as an internal standard, with the methyl signal calibrated at δ 1.2 (^1H) and 31.2 (^{13}C). Spectral assignments were based, in part, on two-dimensional (2D) COSY, HMQC, and HMBC experiments.

Diffusion Coefficient Measurement. The diffusion coefficient of the diamagnetic $[Lu(BPDPA)]^+$ complex (7.83 mM, pD 7.04) was measured in D_2O on a 500 MHz Bruker Avance 500 spectrometer by applying the bipolar-stimulated spin−echo sequence to protons in the

dx.doi.org/10.1021/ic301369z | Inorg. Chem. 2012, 51, 10893−10903

complex.[23] The proton gyromagnetic ratio is denoted by γ_I, the strength of the gradient pulse by g, the duration of this gradient by δ, and the diffusion delay by Δ. The self-diffusion coefficient D_X^t of a species X was calculated by fitting of the theoretical expression of the proton signal intensity $I(\delta,\Delta,g) = I_0 \exp[-(\gamma_I g\delta)^2(\Delta - \delta/3)D_X^t]$, in which $I(\delta,\Delta,g)$ and I_0 are the intensities in the presence and absence of the gradient pulses, respectively. The values chosen for δ and Δ in these measurements depend on the magnitude of the diffusion coefficient being measured. For quickly diffusing HOD molecules, the values of δ and Δ were 2 and 100 ms, respectively. For the slowly diffusing complex, they were 3 and 200 ms, respectively. In the experiments, g was increased from 1.8 to 35.3 G cm^{-1}.

Relaxivity Profiles. Proton NMRD profiles were recorded on a Stelar SMARTracer fast field cycling NMR relaxometer (0.01−10 MHz) and a Bruker WP80 NMR electromagnet adapted to variable field measurements and controlled by a SMARTracer PC-NMR console. The temperature was monitored by a VTC91 temperature control unit and maintained by a gas flow. The temperature was determined by previous calibration with a platinum-resistance temperature probe. The longitudinal relaxation rates ($1/T_1$) were determined in water. The concentration of the $[Gd(BPDPA)]^+$ solution, checked by bulk magnetic susceptibility (BMS) measurements,[24] was 4.08 mM, pH 7.45. The absence of free Gd^{3+} was checked by the xylenol orange test.

Temperature-Dependent ^{17}O NMR Measurements. The transverse ^{17}O relaxation rates ($1/T_2$) and the chemical shifts were measured in aqueous solution in the temperature range 280−350 K, on a Bruker Avance 500 (11.7 T, 67.8 MHz) spectrometer. The temperature was calculated according to previous calibrations with ethylene glycol and methanol.[25] An acidified water solution ($HClO_4$, pH 3.3) was used as the external reference. Transverse relaxation times (T_2) were obtained by the Carr−Purcell−Meiboom−Gill spin−echo technique.[26] The technique of the ^{17}O NMR measurements on Gd^{3+} complexes has been described elsewhere.[27] The samples were sealed in glass spheres fitted into 10 mm NMR tubes to avoid susceptibility corrections of the chemical shifts.[28] To improve the sensitivity, ^{17}O-enriched water (10% $H_2{}^{17}O$, CortecNet) was added to the solutions to reach around 1% enrichment. The concentration of $[Gd(BPDPA)]^+$, checked by BMS,[24] was 13.27 mM, pH 7.25. The absence of free Gd^{3+} was checked by the xylenol orange test.

The ^{17}O NMR data have been treated according to the Solomon−Bloembergen−Morgan theory of paramagnetic relaxation[2] (see the Supporting Information). The least-squares fits of the ^1H NMRD and ^{17}O NMR data were performed using Micromath Scientist, version 2.0 (Salt Lake City, UT). The reported errors correspond to 2 times the standard deviation.

Potentiometric Measurements. The stock solutions of $LnCl_3$ were prepared from $LnCl_3{\cdot}xH_2O$. The concentrations of the solutions were determined by complexometric titration with a standardized Na_2H_2EDTA solution (H_4EDTA = ethylenediaminetetraacetic acid) using xylenol orange as the indicator. Ligand stock solutions were prepared in double-distilled water. The concentration of the ligand in the stock solution as well as the amount of excess acid in the sample (C_{H^+}/C_L) was determined by pH-potentiometric titration. For concentration determinations, solutions of the ligand were titrated with a KOH solution in the absence and presence of a large excess of Ca^{II} ($C_{Ca^{II}}/C_L$ ratio was approximately 50), when all dissociable protons dissociate.

The ligand protonation and stability constants of Ln^{III} complexes were determined by pH-potentiometric titration at 25 °C in 0.1 M KCl. As observed for $BP12C4^{2-}$,[15] the stability constants could be determined from direct potentiometric titrations because complex formation was fast. The samples (3−5 mL) were stirred while a constant N_2 flow was bubbled through the solutions. The pH of the titration mixture was adjusted by the addition of a known volume of standard aqueous HCl. The titrations were carried out by adding a standardized KOH solution with a Methrom 702 SM Titrino automatic burette. A Metrohm 692 pH/ion meter was used to measure the pH. The H^+ concentration was obtained from the measured pH values using the correction method proposed by Irving et al.[29] The ligand and metal−ligand (1:1) solutions (1.9 mM) were titrated over the range 2.0 < pH < 12.0. The titration data for Ln^{III} complexation were successfully refined assuming the presence of only 1:1 metal−ligand species in solution; in all cases, only data corresponding to the lower portions of the titration curves were employed for the calculations in order to avoid complications arising from competing hydrolysis/precipitation at higher pH values. The protonation and stability constants were calculated from parallel titrations with the program *PSEQUAD*.[30] The errors given correspond to 1 standard deviation.

Chemicals and Starting Materials. 2,11-Diaza[3.3](2,6)-pyridinophane (**1**)[31] and 6-(chloromethyl)pyridine-2-carboxylic acid methyl ester (**2**)[16] were prepared according to literature methods. All other chemicals were purchased from commercial sources and used without further purification, unless otherwise stated. Neutral Al_2O_2 (Sigma-Aldrich, Brockmann 1, 150 mesh) was used for preparative column chromatography.

***N,N′*-Bis[(6-methoxycarbonyl-2-pyridyl)methyl]-2,11-diaza-[3.3](2,6)pyridinophane (3).** A mixture of **1** (0.293 g, 1.22 mmol) and diisopropylethylamine (1.48 g, 11.5 mmol) in acetonitrile (60 mL) was heated to reflux for 30 min, and then **2** (0.452 g, 2.44 mmol) and catalytic KI dissolved in acetonitrile (15 mL) were added. The mixture was heated to reflux with stirring for a period of 48 h and filtered, and the filtrate was concentrated to dryness. The brown oily residue was partitioned into equal volumes (50 mL) of H_2O and $CHCl_3$. The aqueous phase was extracted with $CHCl_3$ (4 × 50 mL), and the combined organic extracts were dried over $NaSO_4$, filtered, and evaporated to dryness. The crude product was purified by using column chromatography (neutral Al_2O_3, $CHCl_3$ to 5% MeOH in $CHCl_3$) to yield 0.373 g of the desired compound as a yellow oil (57%). ^1H NMR (solvent $CDCl_3$, 295 K, 500 MHz): δ 7.93 (m, 2H, py, ^3J = 7.50 Hz), 7.86 (t, 2H, ^3J = 7.74 Hz), 7.75 (m, 2H), 7.68 (m, 2H, ^3J = 7.78 Hz), 7.34 (d, 4H, ^3J = 7.74 Hz), 4.57 (s, 8H), 4.35 (s, 4H), 3.96 (s, 6H). ^{13}C NMR (solvent $CDCl_3$, 295 K, 125.8 MHz): δ 164.3, 151.4, 150.1, 147.4, 139.1, 139.0, 127.9, 125.5, 123.9, 61.7, 60.2, 52.9. MS (ESI^+): m/z 539 ($[C_{30}H_{31}N_6O_4]^+$).

***N,N′*-Bis[(6-carboxy-2-pyridyl)methyl]-2,11-diaza[3.3](2,6)-pyridinophane (H_2BPDPA).** A solution of compound **3** (0.248 g, 0.460 mmol) in 6 M HCl (10 mL) was heated to reflux for 48 h. The mixture was filtered while hot and the filtrate concentrated to dryness. The residue was dissolved in water (5 mL) and the solvent removed in a rotary evaporator. This procedure was repeated four times to give 0.240 g of the desired compound as a brown solid (67%). Anal. Calcd for $C_{28}H_{26}N_6O_4{\cdot}7HCl{\cdot}H_2O$: C, 42.91; H, 4.50; N, 10.72. Found: C, 43.25; H, 4.36; N, 10.41. ^1H NMR (solvent D_2O, 295 K, 500 MHz, pD 1.3): δ 8.48 (m, 2H), 8.16 (d, 2H, ^3J = 7.79 Hz), 8.01 (d, 2H, ^3J = 7.78 Hz), 7.71 (t, 2H, ^3J = 7.78 Hz), 7.13 (d, 4H, ^3J = 7.78 Hz), 4.45 (s, 4H, $-CH_2-$), 4.42 (b, 4H, $-CH_2-$). ^{13}C NMR (solvent D_2O, 295 K, 125.8 MHz, pD 1.3): δ 59.6, 58.5 (secondary C), 122.1, 125.3, 128.9, 142.0, 147.6 (tertiary C), 144.4, 152.2, 155.4, 162.2 (quaternary C). MS (ESI^+): m/z 511 ($[C_{28}H_{27}N_6O_4]^+$).

Computational Methods. All calculations were performed employing hybrid DFT with the B3LYP exchange-correlation functional[32,33] and the *Gaussian 09* package (revision A.02).[34] Full geometry optimizations of the $[Ln(BPDPA)(H_2O)]^+$ (Ln = La, Nd, Gd, Ho, Yb) systems were performed in vacuo by using the effective core potential (ECP) of Dolg et al. and the related [5s4p3d]-GTO valence basis set for the lanthanide atoms[35] and the 6-31G(d) basis set for the carbon, hydrogen, nitrogen, and oxygen atoms. No symmetry constraints have been imposed during the optimizations. The default values for the integration grid ("fine") and the self-consistent-field energy convergence criteria (10^{-8}) were used. The stationary points found on the potential energy surfaces as a result of the geometry optimizations have been tested to represent energy minima rather than saddle points via frequency analysis. The molecular volume of $[Gd(BPDPA)(H_2O)]^+$, defined as the volume inside a contour of 0.001 e $bohr^{-3}$, was calculated by using the volume=tight keyword in *Gaussian 09*.

dx.doi.org/10.1021/ic301369z | *Inorg. Chem.* 2012, 51, 10893−10903

RESULTS AND DISCUSSION

Synthesis of the Ligand. Ligand H_2BPDPA (Scheme 1) was obtained in four steps from 2,6-bis(chloromethyl)pyridine

Scheme 1

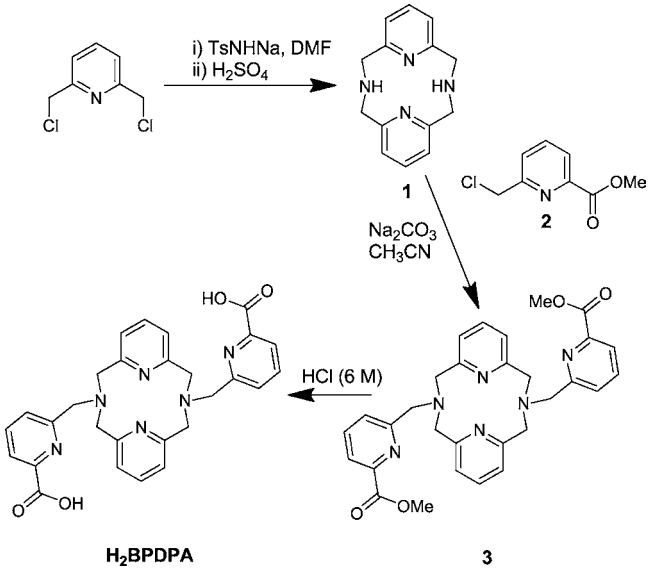

with an overall yield of 22% using the procedure described in the Experimental Section. The synthesis of the diazapyridinophane **1** followed the method described by Bottino et al.,[31] which involves the reaction of 2,6-bis(chloromethyl)pyridine with tosylamide monosodium salt and subsequent deprotection of the tosyl groups under acidic conditions. This method produces a mixture of bis- and tris(pyridine) macrocycles that can be separated by column chromatography. Alkylation of **1** with the 6-(chloromethyl)pyridine derivative **2**[16] in refluxing acetonitrile in the presence of Na_2CO_3 gave compound **3** in 57% yield. Full deprotection of the methyl esters of **3** was cleanly achieved with 6 M HCl to yield the desired ligand H_2BPDPA in good yield (67%).

Photophysical Properties. The absorption spectra of the Eu^{III} and Tb^{III} complexes recorded in water at pH 7.4 (0.1 M MOPS buffer) show a band with a maximum at ca. 263 nm ($\varepsilon \sim 15000\ M^{-1}\ cm^{-1}$) and shoulders at ca. 259, 271, and 278 nm. These absorption maxima can be assigned to a combination of $\pi \rightarrow \pi^*$ and $n \rightarrow \pi^*$ transitions centered on the picolinate moieties and pyridyl units of the macrocyclic fragment (Figure 1).[36] The corresponding emission spectra of ca. 5×10^{-5} M solutions of the Eu^{III} and Tb^{III} complexes, obtained under excitation through the ligand bands at 263 nm, display the $^5D_0 \rightarrow {}^7F_J$ (Eu^{III}, $J = 0-4$) or $^5D_4 \rightarrow {}^7F_J$ (Tb^{III}, $J = 6-3$) transitions characteristic of the particular Ln^{III} ion (Figure 1). The emission spectrum of the Eu^{III} complex is dominated by the $^5D_0 \rightarrow {}^7F_2$ transition, which points to a low symmetry of the ligand field around the Eu^{III} cation.[37] The excitation spectra recorded upon metal-centered emission are very similar to the corresponding absorption spectra, indicating that the coordinated picolinate moieties provide an efficient energy transfer to the Eu^{III} and Tb^{III} ions. The absolute quantum yields of the metal-centered luminescence amount to 1.3% (Eu^{III}) and 16% (Tb^{III}). These data show that pyridyl units of $BPDPA^{2-}$ allow an efficient sensitization of the Tb^{III} luminescence as a result of an efficient ligand-to-metal energy transfer and relatively

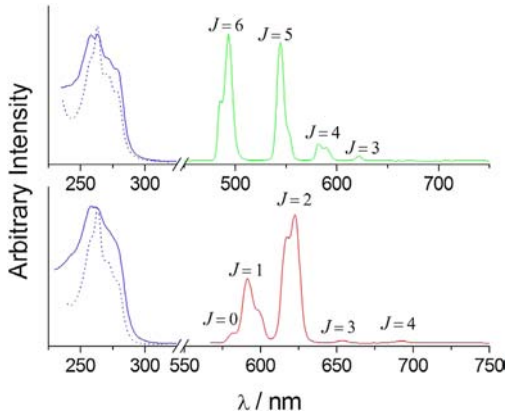

Figure 1. Absorption (dotted lines), excitation, and emission spectra of the Eu^{III} and Tb^{III} complexes of $BPDPA^{2-}$ as recorded in a H_2O solution at room temperature (10^{-5} M, pH 7.4, 0.1 M MOPS).

effective shielding of the metal ion from radiationless deactivation. The quantum yield observed for the Eu^{III} complex is considerably lower than that determined for the Tb^{III} analogue, as is usually observed for Ln^{III} complexes containing picolinate units.[14,15,38]

The emission lifetimes of the Eu($^5D_0$) and Tb($^5D_4$) excited-state levels have been measured in D_2O and H_2O solutions of the complexes and were used to calculate the number of coordinated water molecules q (Table 1). The emission

Table 1. Lifetimes of the Eu($^5D_0$) and Tb($^5D_4$) Excited States of Eu^{III} and Tb^{III} Complexes of $BPDPA^{2-}$, Hydration Numbers (q), and Emission Quantum Yields of the Metal-Centered Emission

complex	λ_{max}/nm	τ_{H_2O}/ms	τ_{D_2O}/ms	q^a	$\Phi(H_2O)$/%
Eu	264	0.66	1.70	0.7	1.3
Tb	263	1.16	1.53	0.7	16

$^a\Delta k_{obs} = k_{obs}(H_2O) - k_{obs}(D_2O)$ and $k_{obs} = 1/\tau_{obs}$. $q_{Eu} = 1.11(\Delta k_{obs} - 0.31)$;[39] $q_{Tb} = 5.0(\Delta k_{obs} - 0.06)$.[40]

lifetimes provide a q value of 0.7 for both the Eu^{III} and Tb^{III} complexes, which points to the presence of one inner-sphere water molecule in solution. The hydration numbers obtained for $[Ln(BPDPA)]^+$ are similar to those obtained for $[Ln(DODPA)]^+$ complexes (Ln = Eu, Tb) but lower than those found for $[Eu(BP12C4)]^+$.[16,18] For the latter complex, UV−vis measurements revealed the presence of an equilibrium in solution involving a 10-coordinated species with $q = 2$ and a 9-coordinated species with $q = 1$, with the average hydration number at 298 K amounting to $q = 1.4$.

Structure of the Complexes in Solution. The ^1H and ^{13}C NMR spectra of the diamagnetic La^{III} and Lu^{III} complexes of $BPDPA^{2-}$ were obtained in D_2O solution at pD 7.0. While for the Lu^{III} complex the spectra are well-resolved at 298 K, in the case of the La^{III} analogue, the ^1H NMR spectrum recorded at room temperature shows broad signals, as was previously observed for the $BP12C4^{2-}$ analogue. The proton spectrum of the Lu^{III} complex consists of 12 signals corresponding to 12 magnetically nonequivalent proton environments in the ligand (see Chart 1 for labeling), pointing to an effective C_2 symmetry of the complex in solution. The most distinctive feature of the ^1H NMR spectrum of $[Lu(BPDPA)(H_2O)]^{2-}$ is the appearance of AB-coupling patterns for the diastereotopic methylene

dx.doi.org/10.1021/ic301369z | Inorg. Chem. 2012, 51, 10893−10903

protons of the macrocyclic unit of the ligand (instead of the singlet observed for the free ligand). Thus, the rapid inversions at the amine nitrogen atoms in the free ligand are revoked by coordination of the ligand to the metal ion.[41] The methylene protons of the pendant arms are also observed as an AB spin system, which indicates a slow interconversion between the Δ and Λ optical isomers arising from the different orientations of the pendant arms.

The assignments of the proton signals (Table 2) were based upon 2D HMQC and HMBC heteronuclear experiments as well as standard 2D homonuclear COSY experiments, which gave strong cross-peaks between the geminal CH_2 protons (4, 5, and 8) and between the ortho-coupled pyridyl protons. Although specific CH_2 proton assignments of the axial and equatorial H4, H5, and H8 protons were not possible on the basis of the 2D NMR spectra, they were carried out using the stereochemically dependent proton shift effects, resulting from polarization of the C−H bonds by the electric field effect caused by the cation charge.[42] This results in a deshielding of the equatorial protons, which are pointing away from the Ln^{III} ion. The signals due to protons H2 and H7 are observed at considerably high fields (δ 6.88 and 7.22, respectively), which is typical of pyridinophanes adopting a syn conformation in solution.[43] This is attributed to the mutual shielding effect on the pyridyl protons caused by the ring current of the other pyridyl unit of the macrocycle.[44]

To obtain information on the solution structure of the Ln^{III} complexes of $BPDPA^{2-}$, we have characterized the $[Ln(BPDPA)(H_2O)]^+$ systems (Ln = La, Nd, Gd, Ho, Lu) by means of DFT calculations (B3LYP model). On the basis of our previous experience,[45] the ECP of Dolg et al.[35] and the related [5s4p3d]-GTO valence basis set were applied in these calculations. The minimum-energy conformation calculated for the $[Gd(BPDPA)(H_2O)]^+$ complex is shown in Figure 2, while selected bond distances and angles of the metal-ion coordination environments are given in Table S1, Supporting Information. The side arms of the ligand are placed above the plane of the macrocyclic unit, resulting in a syn conformation. The syn conformation of the ligand implies that the complexes may exist as two different enantiomeric forms with different orientations of the pendant arms (absolute configurations Δ or Λ).[46,47] The optimized geometries show slightly distorted C_2 symmetries, where the symmetry axis is perpendicular to the pseudoplane described by the four donor atoms of the macrocycle and contains the Ln^{III} ion. The $Gd-O_W$ distance calculated for the $[Gd(BPDPA)(H_2O)]^+$ system (2.596 Å) is somewhat longer than that normally assumed in the analysis of ^{17}O NMR longitudinal relaxation data of nine-coordinated Gd^{III} complexes (2.50 Å). However, this is expected because our DFT calculations were performed in vacuo. In aqueous solution, the $Ln-O_W$ bond distances get shorter because of a stronger water-ion interaction arising from solvent polarization effects upon an increase in the dipole moment of the free water molecules.[48] The distances between the metal ions and donor atoms of the ligand decrease along the lanthanide series, as is usually observed for Ln^{III} complexes as a consequence of the lanthanide contraction.[49]

Table 2. ^1H and ^{13}C NMR Shifts for $[Lu(BPDPA)(H_2O)]^+$ and Comparison of the Experimental and Calculated ^1H NMR Shifts for the $[Yb(BPDPA)(H_2O)]^+$ Complex at 298 K (pD ∼7.0; See Chart 1 for Labeling)

		Yb^{III}			
^1H	Lu^{III} [a]	δ_i^{exp} [b]	δ_i^{calc} [c]	^{13}C	Lu^{III} [a]
H1	7.54	6.19	5.07	C1	142.3
H2	6.88	5.92	5.28	C2	123.3
H4ax	4.21	−2.34	0.07	C3	159.4
H4eq	4.21	13.46	14.38	C4	64.6
H5ax	4.29	38.02	39.80	C5	65.1
H5eq	5.13	25.71	25.63	C6	158.1
H7	7.22	9.94	10.17	C7	124.3
H8ax	4.57	68.52	66.86	C8	63.6
H8eq	5.14	27.54	28.29	C9	159.1
H10	7.89	11.58	10.64	C10	128.4
H11	8.18	3.42	3.03	C11	144.4
H12	7.90	−4.95	−6.02	C12	125.0
				C13	152.2
				C14	174.8

[a]Assignment supported by 2D COSY, NOESY, HMQC, and HMBC experiments at 298 K; $^3J_{2,1}$ = 7.7 Hz; $^2J_{5ax,5eq}$ = 14.4 Hz; $^3J_{7,1}$ = 7.4 Hz; $^2J_{8x,8eq}$ = 15.2 Hz. [b]Assignment supported by 2D COSY experiments at 298 K. [c]Calculated values were obtained using eq 2, and the geometry of the complex was optimized at the B3LYP/6-31G(d) level.

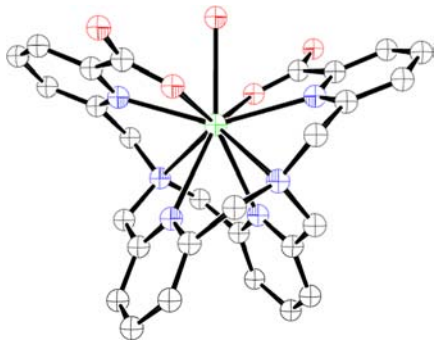

Figure 2. Calculated minimum-energy conformation of $[Gd(BPDPA)(H_2O)]^+$ as optimized in vacuo at the B3LYP/6-31G(d) level. Hydrogen atoms are omitted for the sake of simplicity.

The coordination polyhedron around the Ln^{III} ion in $[Ln(BPDPA)(H_2O)]^+$ complexes may be described as a dodecahedron of C_2 symmetry. The dodecahedron is comprised by two planar trapezoids each defined by the donor atoms of one of the picolinate pendants, the neighboring amine nitrogen atom, and a nitrogen atom of one of the pyridyl units of the macrocycle. The two trapezoids are related by the C_2 symmetry axis of the complex, and the mean deviation from planarity of their mean-square planes amounts to 0.095 Å for the Gd^{III} complex. In $[Gd(BPDPA)(H_2O)]^+$, the two trapezoids intersect at 87.8° (ideal value 90°). The oxygen atom of the inner-sphere water molecule is placed at the C_2 symmetry axis of the complex capping one of the triangular faces of the polyhedron.

The ^1H NMR spectrum of the paramagnetic $[Yb(BPDPA)(H_2O)]^+$ complex is well resolved at room temperature (Figure 3). It shows 12 signals corresponding to the 12 different proton magnetic environments of the ligand (see Chart 1 for labeling), which points to an effective C_2 symmetry of the complex in solution, as was observed previously for the $BP12C4^{2-}$ and $Me\text{-}DODPA^{2-}$ analogues.[16,18] The assignments of the proton signals in $[Yb(BPDPA)(H_2O)]^+$ (Table 2) were based on standard 2D homonuclear COSY experiments, which gave cross-peaks relating to ortho-coupled pyridyl protons, as well as geminal CH_2 protons (4, 5, and 8) and between. The six ^1H

dx.doi.org/10.1021/ic301369z | Inorg. Chem. 2012, 51, 10893−10903

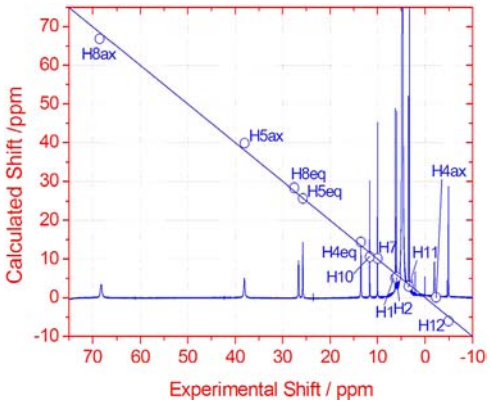

Figure 3. ^{1}H NMR spectrum of $[Yb(BPDPA)(H_2O)]^+$ recorded in a D_2O solution (pD ~7.0) at 298 K and plot of experimental versus calculated shifts. The solid line represents a perfect fit between the experimental and calculated values. See Chart 1 for labeling.

NMR peaks due to protons H4, H5, and H8 can be grouped into two different sets according to their relative line broadening: three resonances with line widths at half-height of 90−175 Hz (at 500 MHz and 298 K) and three signals with line widths in the range of 40−65 Hz (Figure 3). These two sets of signals correspond to two sets of Yb^{III}−proton distances, with the broader resonances being associated with the protons closer to the metal ion.[50] Thus, the broader resonances were assigned to axial protons, while the second set of signals was assigned to equatorial ones.

Aiming to confirm that our DFT calculations provide a good model for the structure of the complexes in solution, we have analyzed the Yb^{III}-induced ^{1}H NMR shifts.[51] The binding of a ligand to a paramagnetic Ln^{III} ion such as Yb^{III} results in large NMR frequency shifts at the ligand nuclei, with magnitudes and signs depending on both the nature of the lanthanide ion and the location of the nucleus relative to the metal center.[52] Thus, analysis of the NMR spectra of Ln^{III} paramagnetic complexes can provide useful structural information in solution. For a given nucleus i, the isotropic paramagnetic shift induced by a lanthanide ion j (δ_{ij}^{para}) is generally a combination of the Fermi contact (δ_{ij}^{con}) and dipolar (δ_{ij}^{dip}) contributions as given in eq 1, where the diamagnetic contribution δ_{ij}^{dia} is obtained by measuring the chemical shifts for analogous diamagnetic complexes (the Lu^{III} complex in the present case).

$$\delta_{ij}^{para} = \delta_{ij}^{exp} - \delta_i^{dia} = \delta_{ij}^{con} + \delta_{ij}^{dip} \quad (1)$$

The hyperfine ^{1}H NMR shifts in Yb^{III} complexes are considered to be largely dipolar in origin, and we therefore initiated analysis of the paramagnetic shifts observed in the ^{1}H NMR spectrum of the Yb^{III} complex with the assumption that they are dominated by the dipolar contribution, which can be written as linear combinations of the five components of the susceptibility tensor χ as given by the following equation:[53]

$$\delta_{ij}^{dip} = \left(\chi_{zz} - \frac{1}{3}\mathrm{Tr}\,\chi\right)\left(\frac{3z^2 - r^2}{r^5}\right) + (\chi_{xx} - \chi_{yy})\left(\frac{x^2 - y^2}{r^5}\right) + \chi_{xy}\left(\frac{4xy}{r^5}\right) + \chi_{xz}\left(\frac{4xz}{r^5}\right) + \chi_{yz}\left(\frac{4yz}{r^5}\right) \quad (2)$$

$$\text{with } r = \sqrt{x^2 + y^2 + z^2} \quad (3)$$

In eq 2, the Cartesian coordinates of atom i relative to the location of a paramagnetic ion are used in place of the more usual spherical coordinates. In the principal magnetic axis system, $\chi_{xy} = \chi_{xz} = \chi_{yz} = 0$, and for axial symmetry, $\chi_{xx} - \chi_{yy} = 0$. According to Neumann's principle,[54] one of the principal magnetic axes of $[Yb(BPDPA)(H_2O)]^+$ must coincide with the 2-fold symmetry axis of the molecule. Thus, we assumed that the z axis of the magnetic susceptibility tensor coincides with the C_2 axis of the molecule. As a consequence, we only considered three (rather than five) parameters in the analysis of the paramagnetic shifts, namely, the axial $[\chi_{zz} - 1/3(\chi_{xx} + \chi_{yy} + \chi_{zz})]$ and rhombic $(\chi_{xx} - \chi_{yy})$ anisotropies of the magnetic susceptibility tensor χ and the orientation of the magnetic axis in the xy plane given by an angle α. The DFT-calculated geometry of the complex was used to assess the agreement between the experimental and predicted Yb^{III}-induced paramagnetic shifts by using a least-squares fit relying on these three parameters. We obtained an excellent agreement between the experimental and calculated shifts (Figure 3; see also Table 2) with $\chi_{zz} - 1/3(\chi_{xx} + \chi_{yy} + \chi_{zz}) = -199 \pm 50$ ppm Å^3 and $\chi_{xx} - \chi_{yy} = 2693 \pm 56$ ppm Å^3. Thus, analysis of the Yb^{III}-induced paramagnetic shifts unambiguously shows that our DFT calculations provide an adequate description of the structure in solution of the complexes investigated in this work.

NMRD and ^{17}O NMR Studies. The relaxivity describes the efficiency of magnetic dipolar coupling occurring between water proton nuclei of the solvent and the paramagnetic metal ion (Gd^{III}) and represents a measure of the efficacy of a contrast agent in vitro. Modulation of the dipolar coupling occurs through rotation of the complex (τ_R), electron magnetic moment relaxation ($T_{1,2e}$), and chemical exchange of the coordinated water molecules with bulk water ($k_{ex} = 1/\tau_M$). The inner-sphere contribution to relaxivity also depends on the number (q) of bound water molecules and their distance (r_{M-H}) from the metal center and on the applied magnetic field strength. Moreover, there is a contribution involving solvent molecules diffusing in the vicinity of the paramagnetic complex (outer-sphere mechanism) that depends on additional parameters: the relative diffusion coefficient of solute and solvent molecules, D, which is the sum of the self-diffusion coefficient of water and the self-diffusion coefficient of the complex, D_S^t, and the distance of closest approach between the solute and solvent molecules, a. NMRD profiles of aqueous solutions of $[Gd(BPDPA)]^+$ were measured at 25, 37, and 50 °C in the proton Larmor frequency range 0.01−80 MHz, corresponding to magnetic field strengths varying between 2.35×10^{-4} and 1.88 T (Figure 4). The relaxivity of $[Gd(BPDPA)]^+$ at 25 and 37 °C is slightly higher than that of $[Gd(DODPA)]^+$, which can be attributed to a slightly higher hydration number of the former. The relaxivity of $[Gd(BPDPA)]^+$ decreases with increasing temperature, indicating that the relaxivity is limited by the fast rotation of the complex in solution rather than by the slow water exchange of the inner-sphere water molecule.

Because of the relatively large number of parameters affecting the relaxivity in Gd^{III} complexes, it is of high importance to determine the maximum of the parameters by independent measurements. First, the self-diffusion coefficient of the complex, D_S^t, can be determined by pulsed-gradient spin−echo ^{1}H NMR, provided that a diamagnetic analogue of the Gd^{3+} complex is used. The self-diffusion coefficient of $[Lu(BPDPA)]^+$ was therefore measured at 298 K in D_2O, $D_S^t(D_2O) = 0.38(1) \times 10^{-9}$ m^2 s^{-1}. This self-diffusion coefficient depends on the solution viscosity η, the van der

dx.doi.org/10.1021/ic301369z | Inorg. Chem. 2012, 51, 10893−10903

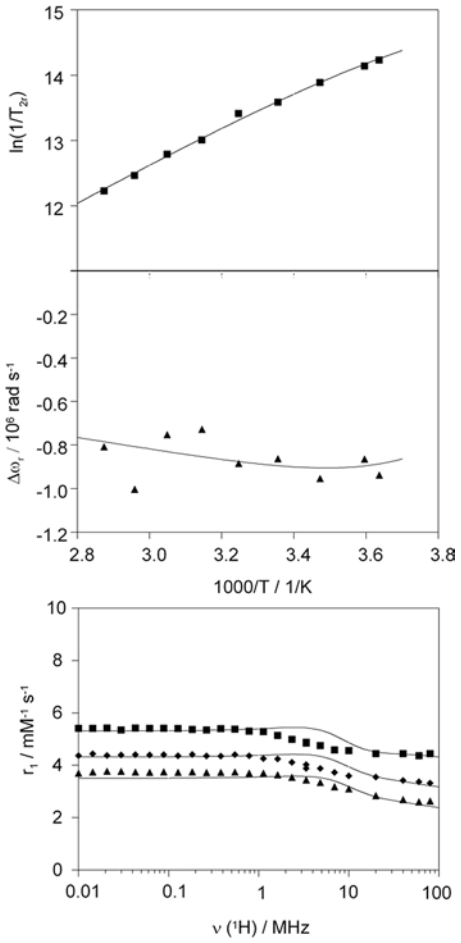

Figure 4. Top: Reduced transverse (■) ^{17}O relaxation rates and ^{17}O chemical shifts (▲) of a $[Gd(BPDPA)]^+$ solution at 11.75 T and neutral pH. Bottom: NMRD profiles recorded for $[Gd(BPDPA)]^+$ at 25 °C (■), 37 °C (◆), and 50 °C (▲). The solid lines represent the fit of the data as described in the text.

Waals radius of the complex a, and a translational microviscosity factor, f_S^t, which accounts for the discrete nature of the solution through the Stokes–Einstein equation, for translation (eq 4).[55]

$$D_S^t = \frac{k_B T}{6\pi a f_S^t \eta} \quad (4)$$

From this equation, we can deduce the value of the self-diffusion coefficient in H_2O, which scales with the viscosity ratio $\eta(D_2O)/\eta(H_2O) = 1.24$ and is calculated to be $D_S^t(H_2O) = 0.47 \times 10^{-9}$ m^2 s^{-1}. The relative diffusion coefficient D can finally be deduced from the self-diffusion coefficient of H_2O, $D_w^t(H_2O) = 2.30 \times 10^{-9}$ m^2 s^{-1},[56] and is found to be $D(H_2O) = 2.77 \times 10^{-9}$ m^2 s^{-1}.

It has become common practice to perform variable-temperature ^{17}O NMR studies of transverse relaxation rates and chemical shits, which depend primarily on $T_{1,2e}$, the hyperfine coupling constant $A/\hbar$, k_{ex}, and q.[57] The reduced transversal relaxation rates obtained for $[Gd(BPDPA)]^+$ (Figure 4) increase with decreasing temperature, which is characteristic of complexes endowed with a fast water-exchange rate of the inner-sphere water molecule, with the observed transversal relaxation rates being dominated by the relaxation rate of the bound water molecule.

A simultaneous fitting of the NMRD and ^{17}O NMR data of $[Gd(BPDPA)]^+$ was performed with the sets of equations given in the Supporting Information. The distance between the proton nuclei of the coordinated water molecule and the Gd^{III} ion (r_{GdH}) was fixed at 3.1 Å,[58] the relative diffusion coefficient was fixed to the experimentally obtained value of 2.77×10^{-9} m^2 s^{-1}, and the number of inner-sphere water molecules in the first coordination sphere was taken as 1.0. The parameters obtained from the simultaneous fitting of the NMRD and ^{17}O NMR data are shown in Table 3, while the results of the fit are given in Figure 4.

It is important to note that the water-exchange rate is not influenced much by the electronic parameters (we checked that reasonable variations of the electronic parameters do not change the water-exchange rate) and can be determined accurately from the fitting of the transverse ^{17}O relaxation rates. It should be emphasized that our fitted parameter for the rotational correlation time τ_R is in very good agreement with the values predicted from the Stokes–Einstein relation for the rotational diffusion constant (eq 5) of the complex.[55] Indeed, the rotational correlation time of a complex τ_R is defined as $\tau_R \equiv 1/6D_S^r$, with

Table 3. Parameters Obtained from Simultaneous Analysis of the ^{17}O NMR and NMRD Data

parameter	$[Gd(DOTA)]^-$ [a]	$[Gd(BP12C4)]^+$ [b]	$[Gd(DODPA)]^+$ [c]	$[Gd(Me\text{-}DODPA)]^+$ [c]	$[Gd(BPDPA)]^+$
q^{298}	1.0	1.4	0.8[c]	0.0[c]	1.0
$k_{ex}^{298}/10^6$ s^{-1}	4.1	220	58		63 ± 6
$\Delta H^{\ddagger}$/kJ mol^{-1}	49.8	14.8	30.7		22 ± 5
$A/\hbar/10^6$ rad s^{-1}	−3.7	−3.4	−2.2		−3.3 ± 0.1
τ_R^{298}/ps	77	105	61.2		83 ± 5
E_r/kJ mol^{-1}	16.1	15	8		15 ± 4
τ_v^{298}/ps	11		15.0	14.9	18 ± 2
$\Delta^2/10^{20}$ s^{-2}	0.16		1.0	1.2	1.3 ± 0.2
E_v/kJ mol^{-1}	1.0		1.5		1.0[d]
$D_{GdH}^{298}/10^{-10}$ m^2 s^{-1}	22		22.4	21.7	27.7[d]
E_{DGdH}/kJ mol^{-1}	20.2		44.8	21.1	35 ± 5
r_{GdH}/Å	3.1		3.168		3.1[d]
a_{GdH}/Å	3.5		4.0	4.1	4.1[d]

[a]Reference 57. [b]Reference 17. [c]Reference 18. [d]Fixed in the fitting procedure.

dx.doi.org/10.1021/ic301369z | Inorg. Chem. 2012, 51, 10893–10903

$$D_S^r = \frac{k_B T}{8\pi a^3 f_S^r \eta} \quad (5)$$

where f_S^r is a microviscosity factor given by

$$f_S^r = \left[\frac{6a_w}{a} + \frac{1 + 3a_w/(a + 2a_w)}{(1 + 2a_w/a)^3}\right]^{-1} \quad (6)$$

with a_w being the water molecule radius with a value of 1.4 Å.

The volume of the $[Gd(BPDPA)]^+$ complex was obtained by means of DFT calculations, defined as the volume inside a contour of 0.001 e bohr^{-3}, and found to be 642.127 Å^3. The radius a of the complex was then evaluated as 5.35 Å by considering a sphere having the same volume. This leads to microviscosity factor f_S^r = 0.50 and rotational correlation time τ_R = 78 ps, which is in excellent agreement with the fitted value (83 ps; Table 3). The value obtained is also consistent with those of $[Gd(DOTA)]^-$, $[Gd(BP12C4)]^+$, and $[Gd(DODPA)]^+$, as expected for complexes of similar size.

The value obtained for the scalar coupling constant $(A/\hbar)$ is similar to those reported for other poly(aminocarboxylate) complexes with one inner-sphere water molecules [typically $(-3.6 \pm 0.3) \times 10^6$ rad s^{-1}],[57,59] which confirms the presence of one inner-sphere water molecule in $[Gd(BPDPA)]^+$. The water-exchange rate is high on $[Gd(BPDPA)]^+$, being at least 1 order of magnitude faster than those for $[Gd(DTPA)]^{2-}$ and $[Gd(DOTA)]^-$ systems,[57] and very similar to that determined for $[Gd(DODPA)]^+$. The highest water-exchange rate observed for $[Gd(BP12C4)]^+$ in comparison to $[Gd(DODPA)]^+$ and $[Gd(BPDPA)]^+$ (ca. 3.7 times faster) may be attributed to an important degree of flexibility of the macrocyclic fragment in $BP12C4^{2-}$ compared to $DODPA^{2-}$ and $BPDPA^{2-}$. The water-exchange rates in $BP12C4^{2-}$, $DODPA^{2-}$, and $BPDPA^{2-}$ complexes are close to the optimal values to attain high relaxivities at intermediate magnetic fields (0.5−1.5 T) provided that τ_R is simultaneously optimized.[60]

Ligand Protonation Constants and Stability Constants of the Ln^{III} Complexes. The protonation constants of $BPDPA^{2-}$ as well as the stability constants of its metal complexes formed with several Ln^{III} ions were determined by potentiometric titrations; the constants and standard deviations are compared to those of related systems in Table 4. The ligand protonation constants are defined in eq 7, and the stability constants of the metal chelates are expressed in eq 8.

$$K_i = \frac{[H_iL]}{[H_{i-1}L][H^+]} \quad (7)$$

$$K_{ML} = \frac{[ML]}{[M][L]} \quad (8)$$

Three protonation constants could be determined for the $BPDPA^{2-}$ ligand. The first two log K values correspond to protonation of the macrocyclic amine nitrogen atoms. Both log K_1 and log K_2 are considerably lower for $BPDPA^{2-}$ than for the bis(acetate) derivative of the same macrocycle (BP2A, Chart 1). This is in agreement with previous observations, which indicated a diminution of the amine basicity upon replacement of the acetate arms by 6-methyl-2-pyridinecarboxylate groups.[62] The third protonation step of $BPDPA^{2-}$ is associated with the carboxylic acid groups.[63]

In order to obtain preliminary information about the rate of complex formation, the ligand (c_{lig} = 1.0 × 10^{-4} M) was mixed with 1 equiv of Eu^{III} at pH 4.2 and the UV−vis spectral changes were recorded in the wavelength range of 225−350 nm after the solutions were mixed with the passing of time (Figure S1, Supporting Information). The spectrum of the ligand changed considerably when the Ln^{III} ion was added to the sample, which is in a good agreement with the rapid formation of an intermediate complex in the initial step. The series of spectra recorded afterward indicate that the formation of the complex is a relatively fast reaction, which was almost complete in 180 s. Thus, the stability constants of the lanthanide complexes of $BPDPA^{2-}$ could be obtained from direct potentiometric titrations.

Table 4. Protonation Constants of $BPDPA^{2-}$ and Related Ligands and Stability Constants of Their Ln^{III} Complexes (25 °C; I = 0.1 M KCl)

	$BPDPA^{2-}$	$BP12C4^{2-}$ [a]	$BP2A^{2-}$ [b]	$DO2A^{2-}$ [c]
log K_1	8.41(6)	9.16	9.57	10.91
log K_2	5.34(7)	7.54	5.99	9.45
log K_3	3.13(8)	3.76	2.59	4.09
log K_4		2.79	2.22	3.18
log K_{LaL}	12.48(3)	16.81		
log K_{CeL}		16.94		
log K_{NdL}	13.32(5)	18.62		
log K_{EuL}				
log K_{GdL}	13.62(7)	18.82	14.5	19.42
log K_{DyL}	14.18(7)	18.11		
log K_{YbL}		18.08		
log K_{LuL}	13.86(8)			

[a]Reference 17. [b]Reference 64. [c]Reference 65.

Analysis of the potentiometric titration data provided the stability constants shown in Table 4. The complex stability increases from the early lanthanides to about the middle of the series and then slightly declines for the heavier lanthanides (Figure 5). In this respect, this chelator is similar to $DTPA^{5-}$ and $BP12C4^{2-}$, in contrast to most of the poly(aminocarboxylate) ligands, such as EDTA, which form complexes of increasing stability all across the lanthanide series because of an increase of the charge density on the metal ions. The stability trend observed for $BPDPA^{2-}$ is also very different from those of $BP18C6^{2-}$ and $BP15C5^{5-}$ (Chart 1),[66] which show an important selectivity for the largest Ln^{III} ions (Figure

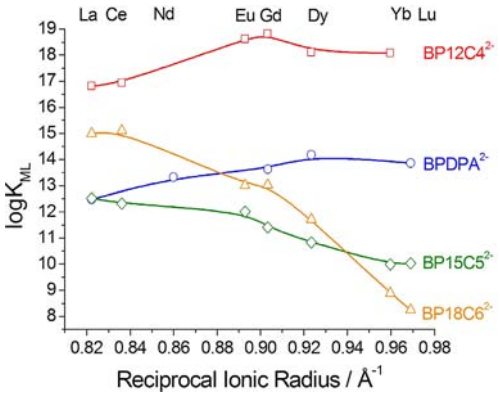

Figure 5. Variation of the stability constants (log K_{ML} values, I = 0.1 M KCl, 25 °C) across the lanthanide series for $BPDPA^{2-}$ complexes and related systems. The solid lines are simply a guide for the eye. Ionic radii were taken from ref 61 assuming coordination number 9.

dx.doi.org/10.1021/ic301369z | Inorg. Chem. 2012, 51, 10893−10903

5). The stability constants determined for $BPDPA^{2-}$ complexes are 4−5 orders of magnitude lower than those of the $BP12C4^{2-}$ analogues, while the stability of the gadolinium complex of $BPDPA^{2-}$ is very similar to that reported for the $BP2A^{2-}$ derivative. The lower stabilities of $BPDPA^{2-}$ complexes compared to $BP12C4^{2-}$ ones can be partially attributed to the lower basicity of the former ligand ($\sum\log\{[H_iBPDPA]/[H_{i-1}BPDPA][H^+]\}$ = 16.9) compared with the latter ($\sum\log\{[H_iBP12C4]/[H_{i-1}BP12C4][H^+]\}$ = 23.3). The effect of the ligand basicity on the stability constants of metal complexes is in line with the stability trend observed for the ligands given in Table 4: $DO2A^{2-}$ > $BP12C4^{2-}$ > $BP2A^{2-}$ > $BPDPA^{2-}$. Besides the effect of the ligand basicity, it has been shown that the preorganized cavity of $BP2A^{2-}$ favors the complexation of small metal ions such as Mg^{2+}. Thus, the relatively low stability constants of Ln^{III} complexes of $BPDPA^{2-}$ are probably also related to a mismatch between the cavity of the diazapyridinophane unit and the large lanthanide ions. Figure S2 (Supporting Information) shows a comparison of the bond distances of the metal-ion coordination environment calculated at the B3LYP level for the $[Ln(BPDPA)(H_2O)]^+$ and $[Ln(BP12C4)(H_2O)]^+$ complexes along the lanthanide series. The bond lengths are generally shorter in $[Ln(BP12C4)(H_2O)]^+$ complexes than in $[Ln(BPDPA)(H_2O)]^+$ ones, which probably reflects the lower basicity of the $BPDPA^{2-}$ ligand and better match between the binding sites offered by the ligand and the large Ln^{III} ions for $BP12C4^{2-}$.

In order to better compare the stability of $[Gd(BPDPA)(H_2O)]^+$ to those of other Gd^{3+} complexes, we have calculated its pGd value at pH 7.4, $c_L = 1 \times 10^{-5}$ M, and $c_{Gd} = 1 \times 10^{-6}$ M (pGd = $-\log [Gd^{3+}]_{free}$).[67] pGd values reflect the influence of the ligand basicity and the protonation of the complex on the stability; the higher the pGd, the more stable the complex under the given conditions. For the Gd^{3+} complex of $BPDPA^{2-}$, we obtain pGd 13.5, a value that is considerably lower than those calculated for $[Gd(DTPA)(H_2O)]^{2-}$ (pGd 19.1) and $[Ln(BP12C4)(H_2O)]^+$ (pGd 17.6) complexes.

CONCLUSIONS

In this work, we have presented the new octadentate ligand $BPDPA^{2-}$, which is based on a diazapyridinophane platform and expands the family of macrocyclic ligands containing picolinate pendant arms reported in previous papers. Luminescence lifetime measurements recorded in H_2O and D_2O solutions of the Eu^{III} and Tb^{III} complexes point to the presence of one water molecule coordinated to the metal ion. NMR data in a D_2O solution and DFT calculations indicate octadentate binding of the ligand through the four donor atoms of the diazapyridinophane unit, the nitrogen atoms of the picolinate pendant arms, and one oxygen atom of a carboxylate function of each pendant arm. Analysis of the Yb^{III}-induced ^1H NMR shifts shows that the structures obtained from DFT calculations are good models for the structure of the complexes in solution. The $[Gd(BPDPA)(H_2O)]^+$ complex maintains the fast water-exchange rate of the inner-sphere water molecule observed previously for the $BP12C4^{2-}$ and $DODPA^{2-}$ derivatives. These water-exchange rates are close to the optimal values required to obtain high relaxivities provided that the rotational correlation time is simultaneously optimized. Furthermore, the terbium complex of $BPDPA^{2-}$ shows a high quantum yield of the metal-centered luminescence. These properties might be of interest for the design of bimodal probes (MRI/optical imaging) combining a high sensitivity and spatial resolution of the two techniques. However, the low basicity of the ligand and a mismatch between the cavity offered by the ligand and the large size of the Ln^{III} ions result in considerably lower complex stabilities for the complexes of $BPDPA^{2-}$ compared to the $BP12C4^{2-}$ analogues.

ASSOCIATED CONTENT

Supporting Information

Optimized Cartesian coordinates (Å) of the complexes investigated in this work, main geometrical parameters of the minimum-energy conformations calculated at the B3LYP/6-31G(d) level, UV−vis spectra showing the formation of the Eu^{3+} complex, and set of equations used for analysis of the NMRD and ^{17}O NMRD data. This material is available free of charge via the Internet at http://pubs.acs.org.

AUTHOR INFORMATION

Corresponding Author

*E-mail: mayter@udc.es (T.R.-B.), carlos.platas.iglesias@udc.es (C.P.-I.).

Notes

The authors declare no competing financial interest.

ACKNOWLEDGMENTS

A.R.-S., D.E.-G., A.d.B., T.R.-B., and C.P.-I. thank the Ministerio de Educación y Ciencia (MEC; Grant CTQ2009-10721), Fondo Europeo de Desarrollo Regional (FEDER; Grant CTQ2009-10721), and Xunta de Galicia (Grant CN2012/011) for financial support. A.R.-S. thanks Xunta de Galicia (the Maria Barbeito program) for a predoctoral fellowship. The authors are indebted to Centro de Supercomputación de Galicia (CESGA) for providing the computer facilities. We also thank Agnès Pallier for performing some NMRD and ^{17}O experiments.

REFERENCES

(1) (a) Bünzli, J.-C. G. *Chem. Rev.* **2010**, *110*, 2729−2755. (b) dos Santos, C. M. G.; Harte, A. J.; Quinn, S. J.; Gunnlaugsson, T. *Coord. Chem. Rev.* **2008**, *252*, 2512−2527. (c) Natrajan, L. S. *Curr. Inorg. Chem.* **2011**, *1*, 61−75. (d) Brunet, E.; Huanes, O.; Rodríguez-Ubis, J. C. *Curr. Chem. Biol.* **2007**, *1*, 11−39. (e) Charbonniere, L. J. *Curr. Inorg. Chem.* **2011**, *1*, 2−16. (f) Xu, J.; Corneillie, T. M.; Moore, E. G.; Law, G.-L.; Butlin, N. G.; Raymond, K. N. *J. Am. Chem. Soc.* **2011**, *133*, 19900−19910.

(2) *The Chemistry of Contrast Agents in Medical Magnetic Resonance Imaging*; Merbach, A. E., Tóth, É., Eds.; Wiley: New York, 2001.

(3) (a) Caravan, P.; Ellinson, J. J.; McMurry, T. J.; Lauffer, R. B. *Chem. Rev.* **1999**, *99*, 2293−2352. (b) Chan, K. W.-Y.; Wong, W.-T. *Coord. Chem. Rev.* **2007**, *251*, 2428−2451. (c) Terreno, E.; Delli Castelli, D.; Viale, A.; Aime, S. *Chem. Rev.* **2010**, *110*, 3019−3042.

(4) Cheng, S.; Abramova, L.; Saab, G.; Turabelidze, G.; Patel, P.; Arduino, M.; Hess, T.; Kallen, A.; Jhung, M. *JAMA* **2007**, *297*, 1542−1544.

(5) Brücher, E.; Sherry, A. D. Stability and Toxicity of Contrast Agents. In *The Chemistry of Contrast Agents in Medical Magnetic Resonante Imaging*; Tóth, E., Merbach, A. E., Eds.; Wiley: Chichester, U.K., 2001; pp 243−279.

(6) (a) Alpha, B.; Lehn, J.-M.; Mathis, G. *Angew. Chem., Int. Ed.* **1987**, *26*, 266−267. (b) Alpha, B.; Ballardi, R.; Balzani, V.; Lehn, J.-M.; Perathoner, S.; Sabbatini, N. *Photochem. Photobiol.* **1990**, *52*, 299−306.

(7) Latva, M.; Takalo, H.; Mukkala, V.-M.; Matachescu, C.; Rodriguez-Ubis, J. C.; Kankare, J. *J. Lumin.* **1997**, *75*, 149−169.

(8) Horrocks, W. D., Jr.; Bolender, J. P.; Smith, W. D.; Supkowski, R. M. *J. Am. Chem. Soc.* **1997**, *119*, 5972−5973.

(9) Pérez-Mayoral, E.; Negri, V.; Soler-Padrós, J.; Cerdán, S.; Ballesteros, P. *Eur. J. Radiol.* **2008**, *67*, 453−458.
(10) Angelovski, G.; Mamedov, I. *Curr. Inorg. Chem.* **2011**, *1*, 76−90.
(11) (a) Werner, E. J.; Datta, A.; Jocher, C. J.; Raymond, K. N. *Angew. Chem., Int. Ed.* **2008**, *47*, 8568−8580. (b) Aime, S.; Botta, M.; Terreno, E. *Adv. Inorg. Chem.* **2005**, *57*, 173−237.
(12) Pellegatti, L.; Zhang, J.; Drahos, B.; Villette, S.; Suzenet, F.; Guillaumet, G.; Petoud, S.; Tóth, É. *Chem. Commun.* **2008**, 6591−6593.
(13) (a) Tallec, G.; Fries, P. H.; Imbert, D.; Mazzanti, M. *Inorg. Chem.* **2011**, *50*, 7943−7945. (b) Tallec, G.; Imbert, D.; Fries, P. H.; Mazzanti, M. *Dalton Trans.* **2010**, *39*, 9490−9492. (c) Caillé, F.; Bonnet, C. S.; Buron, F.; Villette, S.; Helm, L.; Petoud, S.; Suzenet, F.; Tóth, É. *Inorg. Chem.* **2012**, *51*, 2522−2532. (d) Bonnet, C. S.; Buron, F.; Caillé, F.; Shade, C. M.; Drahos, B.; Pellegatti, L.; Zhang, J.; Villette, S.; Helm, L.; Pichon, C.; Suzenet, F.; Petoud, S.; Tóth, É. *Chem.—Eur. J.* **2012**, *18*, 1419−1431. (e) Dehaen, G.; Eliseeva, S. V.; Kimpe, K.; Laurent, S.; Vander Elst, L.; Muller, R. N.; Dehaen, W.; Binnemans, K.; Parac-Vogt, T. N. *Chem.—Eur. J.* **2012**, *18*, 293−302. (f) Placidi, M. P.; Engelmann, J.; Natrajan, L. S.; Logothetis, N. K.; Angelovski, G. *Chem. Commun.* **2011**, *47*, 11534−11536. (g) Bonnet, C. S.; Tóth, É. *C. R. Chim.* **2010**, *13*, 700−714. (h) Laurent, S.; Vander Elst, L.; Wautier, M.; Galaup, C.; Muller, R. N.; Picard, C. *Bioorg. Med. Chem. Lett.* **2007**, *17*, 6230−6233.
(14) (a) Nonat, A.; Gateau, C.; Fries, P. H.; Mazzanti, M. *Chem.—Eur. J.* **2006**, *12*, 7133−7150. (b) Chatterton, N.; Bretonniere, Y.; Pecaut, J.; Mazzanti, M. *Angew. Chem., Int. Ed.* **2005**, *44*, 7595−7598. (c) Nonat, A. M.; Gateau, C.; Fries, P. H.; Helm, L.; Mazzanti, M. *Eur. J. Inorg. Chem.* **2012**, 2049−2061. (d) Nocton, G.; Nonat, A.; Gateau, C.; Mazzanti, M. *Helv. Chim. Acta* **2009**, *92*, 2257−2273.
(15) Regueiro-Figueroa, M.; Bensenane, B.; Ruscsak, E.; Esteban-Gómez, D.; Charbonniere, L. J.; Tircso, G.; Toth, I.; de Blas, A.; Rodriguez-Blas, T.; Platas-Iglesias, C. *Inorg. Chem.* **2011**, *50*, 4125−4141.
(16) Mato-Iglesias, M.; Roca-Sabio, A.; Pálinkás, Z.; Esteban-Gómez, D.; Platas-Iglesias, C.; Tóth, É.; de Blas, A.; Rodríguez-Blas, T. *Inorg. Chem.* **2008**, *47*, 7840−7851.
(17) Palinkas, Z.; Roca-Sabio, A.; Mato-Iglesias, M.; Esteban-Gomez, D.; Platas-Iglesias, C.; de Blas, A.; Rodriguez-Blas, T.; Toth, E. *Inorg. Chem.* **2009**, *48*, 8878−8889.
(18) Rodríguez-Rodríguez, A.; Esteban-Gómez, D.; de Blas, A.; Rodríguez-Blas, T.; Fekete, M.; Botta, M.; Tripier, R.; Platas-Iglesias, C. *Inorg. Chem.* **2012**, *51*, 2509−2521.
(19) Balogh, E.; Mato-Iglesias, M.; Platas-Iglesias, C.; Tóth, É.; Djanashvili, K.; Peters, J. A.; de Blas, A.; Rodríguez-Blas, T. *Inorg. Chem.* **2006**, *45*, 8719−8728.
(20) Haas, Y.; Stein, G. *J. Phys. Chem.* **1971**, *75*, 3668−3677.
(21) Nakamaru, K. *Bull. Chem. Soc. Jpn.* **1982**, *55*, 2697−2705.
(22) Olmsted, J. *J. Phys. Chem.* **1979**, *83*, 2581−2584.
(23) Jerschow, A.; Müller, N. *J. Magn. Reson.* **1997**, *125*, 372−375.
(24) Corsi, D. M.; Platas-Iglesias, C.; van Bekkum, H.; Peters, J. A. *Magn. Reson. Chem.* **2001**, *39*, 723−726.
(25) Raiford, D. S.; Fisk, C. L.; Becker, E. D. *Anal. Chem.* **1979**, *51*, 2050−2051.
(26) Meiboom, S.; Gill, D. *Rev. Sci. Instrum.* **1958**, *29*, 688−691.
(27) Micskei, K.; Helm, L.; Brucher, E.; Merbach, A. E. *Inorg. Chem.* **1993**, *32*, 3844−3850.
(28) Hugi, A. D.; Helm, L.; Merbach, A. E. *Helv. Chim. Acta* **1985**, *68*, 508−521.
(29) Irving, H. M.; Miles, M. G.; Pettit, L. *Anal. Chim. Acta* **1967**, *28*, 475−488.
(30) Zékány, L.; Nagypál, I. In *Computation Methods for Determination of Formation Constants*; Leggett, D. J., Ed.; Plenum: New York, 1985; p 291.
(31) Bottino, F.; Di Grazia, M.; Finocchiaro, P.; Fronczek, F. R.; Mamo, A.; Pappalardo, S. *J. Org. Chem.* **1988**, *53*, 3521−3529.
(32) Becke, A. D. *J. Chem. Phys.* **1993**, *98*, 5648−5652.
(33) Lee, C.; Yang, W.; Parr, R. G. *Phys. Rev. B* **1988**, *37*, 785−789.
(34) Frisch, M. J.; Trucks, G. W.; Schlegel, H. B.; Scuseria, G. E.; Robb, M. A.; Cheeseman, J. R.; Scalmani, G.; Barone, V.; Mennucci, B.; Petersson, G. A.; Nakatsuji, H.; Caricato, M.; Li, X.; Hratchian, H. P.; Izmaylov, A. F.; Bloino, J.; Zheng, G.; Sonnenberg, J. L.; Hada, M.; Ehara, M.; Toyota, K.; Fukuda, R.; Hasegawa, J.; Ishida, M.; Nakajima, T.; Honda, Y.; Kitao, O.; Nakai, H.; Vreven, T.; Montgomery, J. A., Jr.; Peralta, J. E.; Ogliaro, F.; Bearpark, M.; Heyd, J. J.; Brothers, E.; Kudin, K. N.; Staroverov, V. N.; Kobayashi, R.; Normand, J.; Raghavachari, K.; Rendell, A.; Burant, J. C.; Iyengar, S. S.; Tomasi, J.; Cossi, M.; Rega, N.; Millam, N. J.; Klene, M.; Knox, J. E.; Cross, J. B.; Bakken, V.; Adamo, C.; Jaramillo, J.; Gomperts, R.; Stratmann, R. E.; Yazyev, O.; Austin, A. J.; Cammi, R.; Pomelli, C.; Ochterski, J. W.; Martin, R. L.; Morokuma, K.; Zakrzewski, V. G.; Voth, G. A.; Salvador, P.; Dannenberg, J. J.; Dapprich, S.; Daniels, A. D.; Farkas, Ö.; Foresman, J. B.; Ortiz, J. V.; Cioslowski, J.; Fox, D. J. *Gaussian 09*, revision A.01; Gaussian, Inc.: Wallingford, CT, 2009.
(35) Dolg, M.; Stoll, H.; Savin, A.; Preuss, H. *Theor. Chim. Acta* **1989**, *75*, 173−194.
(36) Renaud, F.; Piguet, C.; Bernardelli, G.; Bünzli, J.-C. G.; Hopfgartner, G. *Chem.—Eur. J.* **1997**, *3*, 1646−1659.
(37) Görller-Walrand, C.; Binnemans, K. In *Handbook on the Physics and Chemistry of Rare Earths*; Gschneider, K. A., Jr., Eyring, L., Eds.; Elsevier Science: Amsterdam, The Netherlands, 1998; Vol. *25*, p 101.
(38) (a) Platas-Iglesias, C.; Mato-Iglesias, M.; Djanashvili, K.; Muller, R. N.; Vander Elst, L.; Peters, J. A.; de Blas, A.; Rodríguez-Blas, T. *Chem.—Eur. J.* **2004**, *10*, 3579−3590.
(39) Supkowski, R. M.; Horrocks, W. D., Jr. *Inorg. Chim. Acta* **2002**, *340*, 44−48.
(40) Beeby, A.; Clarkson, I. M.; Dickins, R. S.; Faulkner, S.; Parker, D.; Royle, L.; de Sousa, A. S.; Williams, J. A. G.; Woods, M. *J. Chem. Soc., Perkin Trans. 2* **1999**, 493−503.
(41) Kelm, H.; Krüger, H.-J. *Inorg. Chem.* **1996**, *35*, 3533−3540.
(42) Harris, R. K. *Nuclear Magnetic Resonance Spectroscopy: A Physicochemical View*; Pitman: London, 1983.
(43) Newkome, G. R.; Pappalardo, S.; Fronczek, F. R. *J. Am. Chem. Soc.* **1983**, *105*, 5152−5153.
(44) McConnell, H. M. *J. Chem. Phys.* **1957**, *27*, 226−229.
(45) Platas-Iglesias, C.; Roca-Sabio, A.; Regueiro-Figueroa, M.; Esteban-Gómez, D.; de Blas, A.; Rodríguez-Blas, T. *Curr. Inorg. Chem.* **2011**, *1*, 91−116.
(46) Corey, E. J.; Bailar, J. C., Jr. *J. Am. Chem. Soc.* **1959**, *81*, 2620−2629.
(47) Beattie, J. K. *Acc. Chem. Res.* **1971**, *4*, 253−259.
(48) Djanashvili, K.; Platas-Iglesias, C.; Peters, J. A. *Dalton Trans.* **2008**, 602−607.
(49) Seitz, M.; Oliver, A. G.; Raymond, K. N. *J. Am. Chem. Soc.* **2007**, *129*, 11153−11160.
(50) Aime, S.; Barbero, L.; Botta, M.; Ermondi, G. *J. Chem. Soc., Dalton Trans.* **1992**, 225−228.
(51) Platas-Iglesias, C. *Eur. J. Inorg. Chem.* **2012**, 2023−2033.
(52) Peters, J. A.; Huskens, J.; Raber, D. J. *Prog. NMR Spectrosc.* **1996**, *28*, 283−350.
(53) Forsberg, J. H.; Delaney, R. M.; Zhao, Q.; Harakas, G.; Chandran, R. *Inorg. Chem.* **1995**, *34*, 3705−3715.
(54) Terazzi, E.; Rivera, J.-P.; Ouali, N.; Piguet, C. *Magn. Reson. Chem.* **2006**, *44*, 539−552.
(55) Rast, S.; Fries, P. H. *J. Chem. Phys.* **2000**, *113*, 8724−8735.
(56) Holz, M.; Weingärtner, H. *J. Magn. Reson.* **1991**, *92*, 115−125.
(57) Powell, H. D.; Ni Dhubhghaill, O, M.; Pubanz, D.; Helm, L.; Lebedev, Y.; Schlaepfer, W.; Merbach, A. E. *J. Am. Chem. Soc.* **1996**, *118*, 9333.
(58) Astashkin, A. V.; Raitsimring, A. M.; Caravan, P. *J. Phys. Chem. A* **2004**, *108*, 1990−2001.
(59) Alpoim, M. C.; Urbano, A. M.; Geraldes, C. F. G. C.; Peters, J. A. *J. Chem. Soc., Dalton Trans.* **1992**, 463−467.
(60) Caravan, P.; Farrar, C. T.; Frullano, L.; Uppal, R. *Contrast Media Mol. Imaging* **2009**, *4*, 89−100.
(61) Shannon, R. D. *Acta Crystallogr.* **1976**, *A32*, 751−767.

(62) Chatterton, N.; Gateau, C.; Mazzanti, M.; Pecaut, J.; Borel, A.; Helm, L.; Merbach, A. *Dalton Trans.* **2005**, 1129−1135.
(63) (a) Ferreiros-Martinez, R.; Esteban-Gomez, D.; Platas-Iglesias, C.; de Blas, A.; Rodriguez-Blas, T. *Dalton Trans.* **2008**, 5754−5765. (b) Pellissier, A.; Bretonniere, Y.; Chatterton, N.; Pecaut, J.; Delangle, P.; Mazzanti, M. *Inorg. Chem.* **2007**, *46*, 3714−3725.
(64) Kim, W. D.; Hrncir, D. C.; Kiefer, G. E.; Sherry, A. D. *Inorg. Chem.* **1995**, *34*, 2225−2232.
(65) (a) Lacoste, R. G.; Christoffers, G. V.; Martell, A. E. *J. Am. Chem. Soc.* **1965**, *87*, 2385−2388. (b) Martell, A. E.; Motekaitis, R. J.; Smith, R. M. *NIST Critically Selected Stability Constants of Metal Complexes Database*; Standard Reference Data Program, Version 8.0 for Windows; National Institute of Standards and Technology: Gaithersburg, MD, 2004.
(66) (a) Roca-Sabio, A.; Mato-Iglesias, M.; Esteban-Gomez, D.; de Blas, A.; Rodriguez-Blas, T.; Platas-Iglesias, C. *Dalton Trans.* **2011**, *40*, 384−392. (b) Roca-Sabio, A.; Mato-Iglesias, M.; Esteban-Gomez, D.; Toth, E.; de Blas, A.; Platas-Iglesias, C.; Rodriguez-Blas, T. *J. Am. Chem. Soc.* **2009**, *131*, 3331−3341.
(67) Harris, W. R.; Carrano, C. J.; Raymond, K. N. *J. Am. Chem. Soc.* **1979**, *101*, 2213−2214.